UNCONVENTIONAL RESOURCES TECHNOLOGY CONFERENCE
FUELED BY SPE • AAPG • SEG

URTeC: 2902986

Determining the Impact of Mineralogy Composition for Multiphase Flow through Hydraulically Induced Fractures

Javier E. Santos*[1], Maša Prodanović[1], Christopher J. Landry[2], Honggeun Jo[1]
[1]Hildebrand Department of Petroleum and Geosystems Engineering, The University of Texas at Austin. [2]Center for Petroleum and Geosystems Engineering, The University of Texas at Austin.

Abstract

Hydraulic fracturing techniques aim to create high conductivity channels through low permeability rocks, enhancing hydrocarbon flow to the wellbore. However, characterizing the reduction of mobility in fractures as a result of surface heterogeneities, has received limited attention. In this work, we study the effect of the heterogeneity in composition and roughness in flow through hydraulically induced fractures. Since analytical solutions are restricted to simple domains, a 3D direct simulation approach was selected. To assess these effects, domains exhibiting geometrical mineral arrangements, and self-affine fractures were created to carry out drainage and imbibition simulations. The relations of different wetting/non-wetting patterns and surface roughness, with interfacial areas, capillary pressure, and residual fluid saturation were quantified. We show that there is an effective mineral feature size related to the fracture dimensions that modifies the capillary pressure behavior. Similarly, the correlation range of the surface apertures determines the effect of the shape of a non-wetting front. Correspondingly, we found that for increasingly rough surfaces, there is a linear relation between the residual non-wetting saturation and capillary pressure with the aperture distribution. Thus, the shape, mineral size ratio, and surface roughness can have a significant effect on flow patterns. The results of this work can be used to improve macroscopic simulations, having a priori knowledge of the microscopic characteristics.

1. Introduction

Open fractures in subsurface formations represent preferential channels for fluid flow. At the field scale, these geological elements are described using dual porosity/permeability continuum models (Bear, 1993). Fracture apertures and lengths span multiple orders of magnitude (Brown & Scholz, 1985; Gale et al., 2007), and while these models can work for larger scales, they are not applicable for characterizing flow at the pore scale. Such fractures, often partially lined with mineral cements, can have a large impact on flow in unconventional reservoirs (Gale et al., 2014). These features increase the complexity of the flow paths, yielding in errors when utilizing conventional solutions, by not accounting for different mineralogy (Iglauer et al., 2015) or phase trapping (Tokan-Lawal et al., 2014). However, presently we do not have enough pore scale studies to fully understand how flow processes act with the different heterogeneities present in natural fractures. The present work focuses on correlating different mineral arrangements, fracture aperture, and surface roughness for imbibition and drainage experiments.

Fractures are commonly modeled using simplified solutions (i.e. parallel plates, straight relative permeability curves), where natural surface complexities are not taken into account. It has been demonstrated, that the predictions made with these can vary by orders of magnitude (Tokan-Lawal et al., 2015), and provide an oversimplified view of the complex multiphase flow phenomena. Studies have shown that the multiphase displacement, specifically phase trapping, through fractures resembles porous medium matrix behavior (Piri & Karpyn, 2007; Prodanovic & Bryant,

DOI:10.15530/urtec-2018-2902986

2009). Further, models that take into account a surface heterogeneous composition, only work for simple problems. Cassie (1948) proposed a relationship to calculate an effective contact angle on a flat surface with two distinct minerals (labeled 1 and 2):

$$\cos\theta_{eff} = f_1 cos\theta_1 + f_2 cos\theta_2$$

where θ stands for the contact angle, and f for the areal fraction covered by it. This expression assumes that the most relevant parameter is the areal fraction occupied by a certain mineral. Other studies suggest that the contact angle is shaped by the interactions that occur at the triple-point (Li et al., 2016). Further work studied the validity of the Cassie equation, but limited to a single droplet (Dupuis & Yeomans, 2004; Iwahara et al., 2003; Kusumaatmaja & Yeomans, 2007; Zhang, Li, & Kwok, 2009). Another difficulty that is faced while modeling these processes, is the variable wettability of the minerals in presence of reservoir fluids (Tokunaga & Wan, 2013); it has been shown that a system (i.e. quartz/CO_2/brine) can exhibit contact angles ranging from 0 to 90 degrees (Iglauer et al., 2015).

Initial studies in fractures (Romm, 1966) suggested that the relative permeability curve has a linear dependency with fluid saturation. However, later studies (Pruess & Tsang, 1990) showed that roughness plays an important role, and that the relationships are non-linear. In rough and constricted fractures, multiphase flow will have similarities with pore scale flow in the matrix (Piri & Karpyn, 2007). Hassanizadeh and Gray (1993) theoretically explained that knowing the interface distribution and length is critical to describe the capillary pressure-saturation relation of a porous medium, and to explain the hysteresis in the curves. Several studies have shown that capillary pressure depends on several factors, including the history of imbibition and drainage cycles, injection rate, among others. There have been published attempts to quantify the effect of different interfacial configurations (Cheng et al., 2004).

Fracture roughness can be quantified through a fractal dimension D_f (Mandelbrot, 1983), which measures the topological complexity of an object (0 for a point, 1 for a curve, 2 for a surface), and a related measure is the Hurst exponent H (where: $D_f + H = 3$) (Gneiting & Schlather, 2001). Furthermore, fractures are spatially correlated, though it is not a straightforward parameter to measure. Brown (1995) presented a model to describe the fracture surfaces that included a 'mismatch length' term that defined the scale on which the surfaces were correlated. Later, Ogilvie et al. (2006) improved the model by adding a 'transition length' parameter to account for the speed of the wavelength match, and successfully parametrized and recreated several natural fractures on different lithology.

Characterizing fractures using a fractal dimension and a spatial correlation of the bounding surfaces is a common practice to describe real fractures (from faults spanning km., to microfractures). In this paper, we provide a study that assesses the main variables that control multiphase flow through these geometries, while providing a full characterization of the studied fractures. For this study, we selected the lattice-Boltzmann method (LBM) based on its ability to simulate flow through complex geometries, its highly parallelizable engine, and its kinetic theory consistency. To further investigate multiphase flow, the Shan-Chen (Shan & Chen, 1993; Shan & Chen, 1994) lattice-Boltzmann model was chosen based on its capability to simulate multiple phases that honor the properties of an oil-brine system, and its capacities of handling complex boundary conditions. Other options include quasi-static level set methods (Jettestuen et al., 2013; Verma et al., 2018), although these do not take in account viscous forces, or volume of fluid methods which prove more complicated to implement (Raeini et al., 2012). Previously, the Shan-Chen (SC) LBM has been used to study flow through porous matrix; Pan et al. (2004) simulated displacement experiments on a sphere-pack that matched well with experimental results, proving that this model is a feasible technique to study multiphase flow processes. In the context of fractured media, Dou et al. (2013) showed how homogeneous rough fractures with different contact angle impact the unsteady-state capillary pressure curves. Landry et al. (2014) studied how the heterogeneous composition of a bead pack adversely affected the relative permeability compared with homogenous-wet states. To our knowledge, this work provides the first effort to characterize heterogeneous, roughly-composed fracture surfaces with a direct simulation approach.

2. Methods

2.1 The Lattice-Boltzmann Method

To carry out the simulations, the lattice-Boltzmann method (LBM) was selected based on its ability to handle realistic geometries, and complex wall boundary conditions. The LBM relies on discrete momentum distributions to represent particle movement, where the domain is divided in nodes that host particles propagating and interacting with their nearest neighbors. Unlike molecular dynamics simulations, the LBM does not track individual molecules, but relies on the density of the bulk fluid. Using this, it is possible to calculate macroscopic variables like fluid density and velocity. The particle function *f* satisfies the following lattice-Boltzmann equation:

$$f_i(x,t) - f_i(x + e_i\Delta t, t + \Delta t) = \frac{1}{\tau}\left(f_i(x,t) - f_i^{eq}(x,t)\right)$$

Where the subscript *i* stands for the index of the associated discrete velocity (e) direction, *x* is the location of the node on the lattice, *t* is the time, τ is the relaxation time (rate of particle collisions), and f^{eq} the equilibrium particle distribution function. The left side of the equation represents the passing of particles to their respective neighboring node at each discrete velocity (streaming), whereas the right side refers to a relaxation towards local equilibrium (collision).

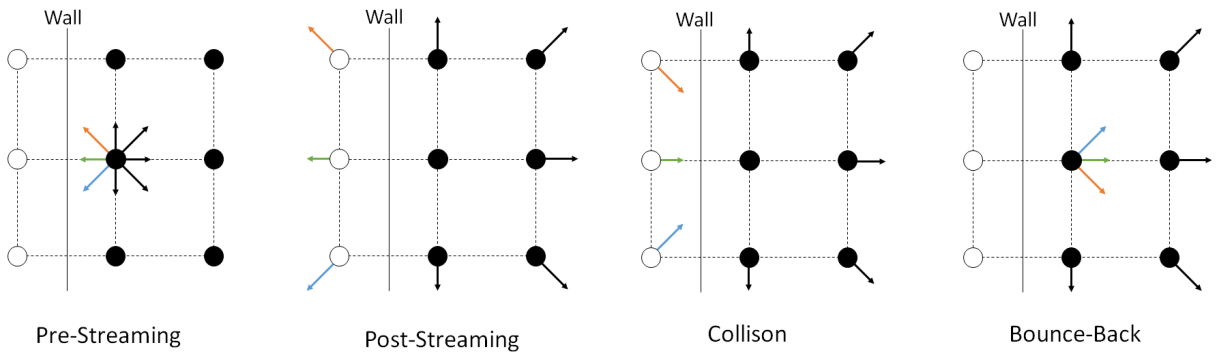

Figure 1: Four stages of the LBM iteration process.

For this work, we chose the three dimensional, 19 discrete velocity model (D3Q19). To estimate the collision term, we use the Bhatnagar-Gross-Krook single relaxation time (Bhatnagar, Gross, & Krook, 1954) approximation. For this case, the equilibrium function is computed utilizing the following equation:

$$f_i^{eq}(x,t) = w_i\rho(1 + \frac{e_i u^{eq}}{c_s^2} + \frac{1}{2}\left(\frac{e_i u^{eq}}{c_s^2}\right)^2 - \frac{1}{2}\left(\frac{u^{eq}}{c_s}\right)^2)$$

Where w_i is the weight of each discrete velocity, ρ the density, u^{eq} the macroscopic velocity, and $c_s = \Delta t/\Delta x/\sqrt{3}$, which is the propagation speed of the lattice. Each discrete velocity is defined as:

	e1	e2	e3	e4	e5	e6	e7	e8	e9	e10	e11	e12	e13	e14	e15	e16	e17	e18	e19
	0	1	-1	0	0	0	0	1	1	-1	-1	1	-1	1	-1	0	0	0	0
(Δx/Δt)	0	0	0	1	-1	0	0	1	-1	1	-1	0	0	0	0	1	1	-1	-1
	0	0	0	0	0	0	1	-1	0	0	0	0	1	1	-1	-1	1	-1	-1

We selected the Shan-Chen (SC) model to carry out the multiphase simulations because of its capability to maintain relatively sharp interfaces, and handling rock-fluid interactions. In the SC model, to simulate a binary fluid system (wetting/non-wetting) each fluid is assigned a distribution function at every node.

The fluids interact via a pseudo-potential (interparticle) force, which is calculated as follows:

$$F_{co,\sigma}(x,t) = -G_c\rho_\sigma(x,t)\sum_i w_i\rho_{\overline{\sigma}}(x + e_i\Delta t, t)e_i$$

Where G_c is the interparticle force. The subscripts $\overline{\sigma}$ and σ represent the two different fluids. To simulate the fluid-solid interaction and adhesion force is introduced as depicted below:

$$F_{ads,\sigma}(x,t) = -G_{ads}\rho_\sigma(x,t)\sum_i w_i e_i \cdot s(x + e_i\Delta t, t)e_i$$

In here, *s* is a Boolean function that is equal to *1* for a bounce back node, and to *0* for a solid node. G_{ads} represents the interaction between the fluid and the solid walls. Huang et al. (2007) proposed the following relation to set the parameters above and obtain the desired contact angle:

$$cos\theta_\sigma = \frac{G_{ads,\overline{\sigma}} - G_{ads,\sigma}}{G_c\,\frac{\rho_\sigma - \rho_{\overline{\sigma}}}{2}}$$

The parameters in the equation above where selected according to recommendations published by Huang et al., (2007).

3 Results

3.1 Numerical Benchmarks

The flow through a homogeneous, parallel, infinite slit was simulated for validating our LBM model. Figure 2 shows the comparison between the analytical solution and the simulation.

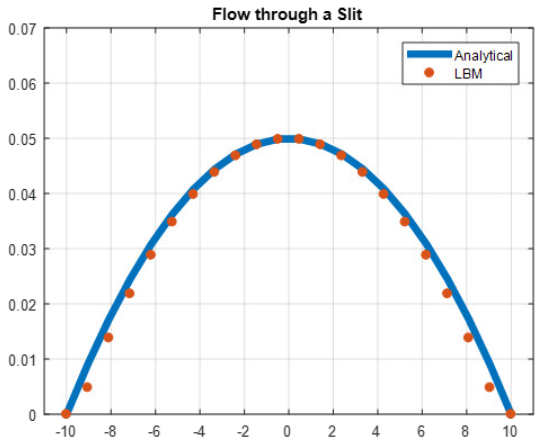

Figure 2: Velocity field comparison of the LBM simulation with the analytical solution (Navier-Stokes) for a slit with aperture of 20 lattice units.

The contact angle of a droplet of fluid on a flat, solid surface (wetting and non-wetting) was measured to assess the surface interaction parameter of our multiphase model (Figure 3). The comparison between the simulation result and the prediction from Young's equation, is presented in the table below:

Table 1: Comparison between the contact angle predicted by Young's equation and our model.

Young's equation [º]	Model [º]
156.4	154.02
23.6	24.1

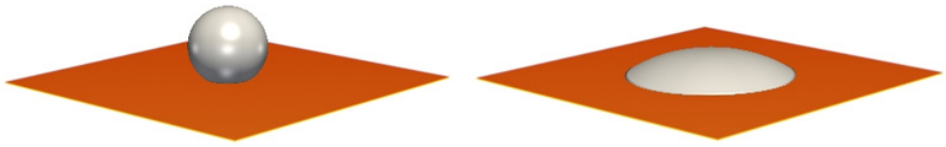

Figure 3: Non-wetting and wetting surfaces. The pictures show the results of our model.

To test the validity of capillary dominated displacement, drainage and imbibition experiments were performed in a domain comprised of aligned capillary tubes (Figure 5). The comparison between the analytical solution (Washburn, 1921), and the results of our model are displayed in Figure 4. For our tests, the capillary number (Lake, Johns, Rossen, & Pope, 2014) was kept under 10^{-6} to ensure capillary dominated displacement.

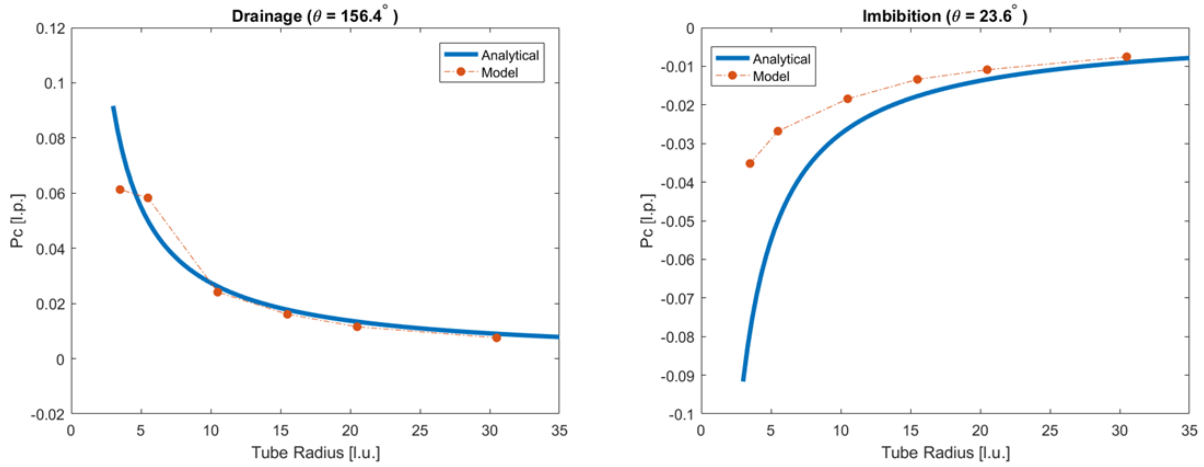

Figure 4: Comparison of drainage (left) and imbibition (right) tests for our model. On the x axis the tube radius in lattice units (voxels) is shown, the y axis describes capillary pressure (the difference between the pressure of the non-wetting phase minus the wetting phase) in lattice units.

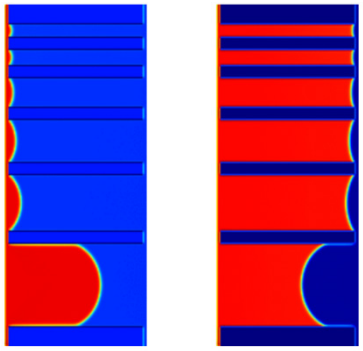

Figure 5: Capillary tubes experiment. On the left, the first tube (largest) is draining (156.4°). To the right the last meniscus is imbibing (23.6°)

3.3 Flow through Heterogeneous Flat Surfaces

Studies suggest that fracture aperture dominates flow processes, nevertheless mineral wettability affects flow patterns. It has been shown, that each mineral has a distinct wettability (as measured by the contact angle) at different scales (Deglint et al., 2017). To evaluate the effect of heterogeneous wettability on flow, a pair of flat plates were used. In this domain, two different mineralogy patterns were simulated. One comprising alternating wetting and non-wetting stripes, and one exhibiting non-wetting disks (Figure 6). In both cases, the wetting and non-wetting areal fractions were kept equal (50% each).

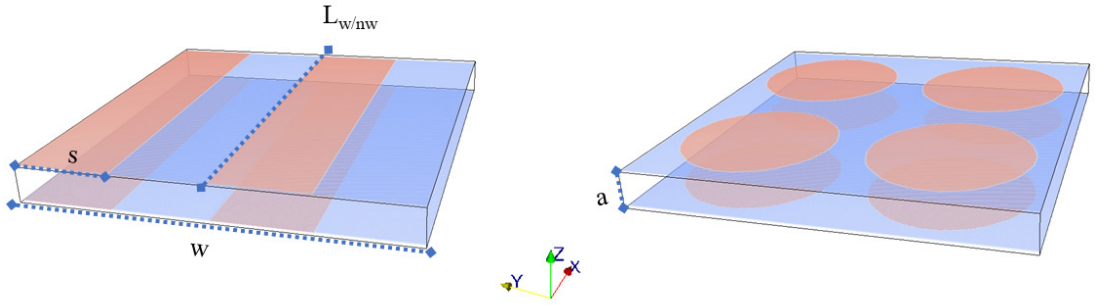

Figure 6: Simulation domains. The red color represents minerals that are wetted by the red fluid, contrariwise the blue color represents minerals wetted by the blue fluid. We introduce the variable $L_{w/nw}$ for the striped fractures, which stands for the length of the intersection between the wetting and non-wetting patches in the solid phase. With w we denote the domain width and with s the length of one of the stripes. The aperture is referred as a.

The aperture (a), number of stripes and number of disks were varied to assess their effect on the invasion front. The domain is initially saturated with the fluid (blue) wetting the blue surface. Using capillary pressure increments a displacing fluid (that wets the red surface) is injected along the y axis. The boundary conditions on the x axis are periodic (infinite).

To normalize the capillary pressure corresponding to different apertures, we introduce a critical pressure term, which stands for the pressure to completely drain wetting fluid from a fracture with homogeneous surface mineralogy with a non-wetting fluid (156.4º), calculated as follows:

$$P_{c,crit} = \frac{2\sigma}{a}\cos(156.4^{\circ})$$

where σ stands for the interfacial tension, and a for the fracture aperture. The contact angle is taken from Table 1.

In the striped domain, capillary fingering was visible under the conditions depicted in Figure 7, where the normalized capillary fingering is shown. From these results, we hypothesize that there is a threshold ratio between aperture and feature length that controls this behavior. To measure these features, a 2D slice was taken in the middle of the domain (z=a/2). These slices are visible on the right-hand side of Figure 7.

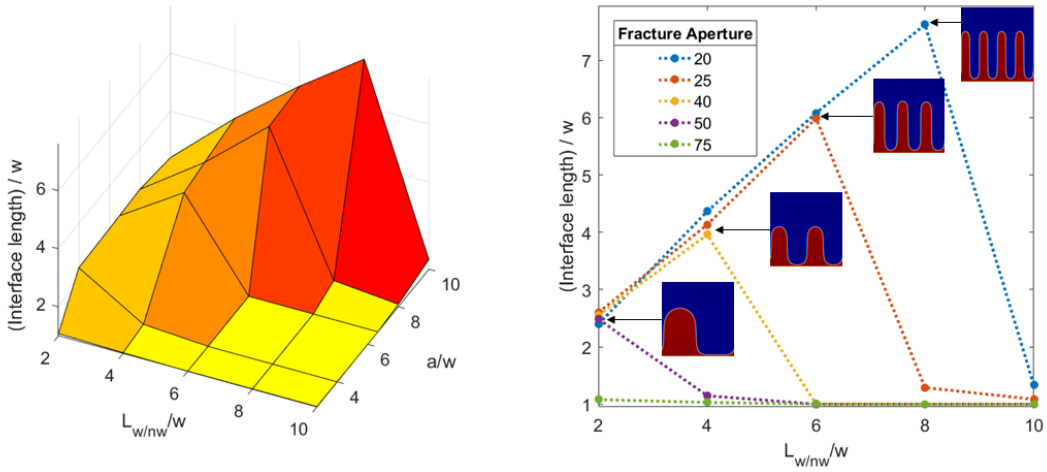

Figure 7: Normalized interfacial length for 25 different cases. Where the number of wetting stripes and the aperture was varied.

Further analysis confirms that a geometric threshold exists in all the cases above. A plot exhibiting this is displayed in Figure 8.

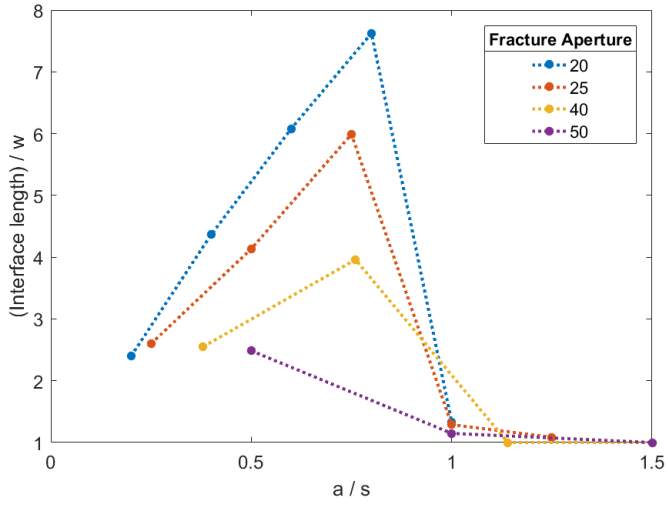

Figure 8: Normalized interfacial length vs the ratio of aperture over the length of the stripe. There is a critical threshold (aperture/(feature length)=1) where the capillary fingering no longer occurs.

From this, it is visible that when the fracture aperture is greater than the length of the heterogeneous feature (stripe in this case), the capillary fingering effects disappear. These anomalies play against capillary pressure predictions calculated with the Young equation, as shown in Figure 9.

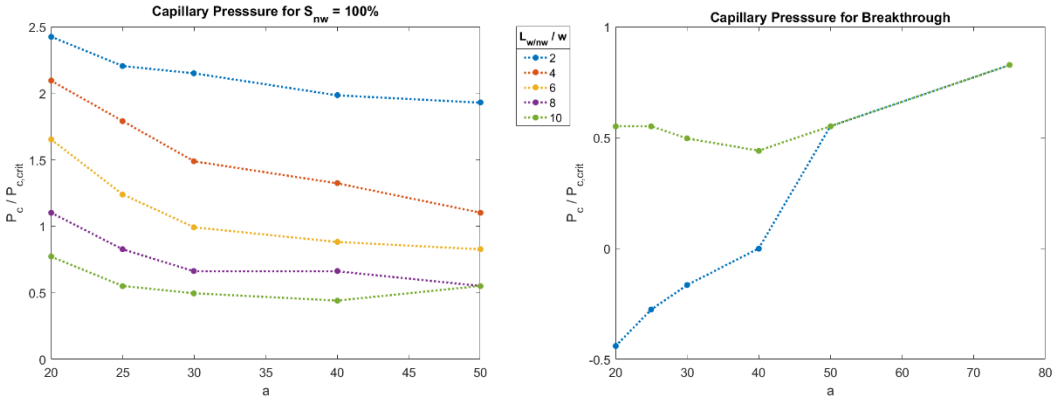

Figure 9: Normalized capillary pressure curves for complete drainage and breakthrough. With different colors, cases with an increasing number of stripes are presented. The capillary pressure was normalized using $P_{c,crit}$, which corresponds to the pressure to drain a completely non-wetting fracture with no stripes. Fingering has an adverse effect on the full drainage curve, exhibiting pressures up to 2.5 times the critical capillary pressure. In the smallest aperture domains, spontaneous imbibition was seen at breakthrough.

To test our hypothesis further, simulations were run in the domain comprised by non-wetting disks. The critical geometrical parameters (similar to the ones presented in Figure 8) are shown in Table 2. The capillary pressure-saturation curve for two different apertures are plot in Figure 10.

Table 2: Critical geometric ratio of the simulations.

Case	a/radius
Blue curve (Figure 10)	0.5
Red curve (Figure 10)	1.25

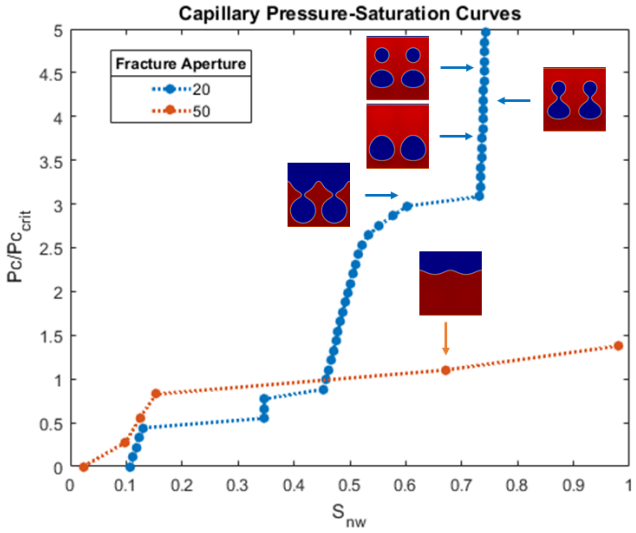

Figure 10: Results of the simulations. On the blue curve, contact line pinning (Jung et al., 1992) occurs when the critical ratio is smaller than 1.

3.4 Flow through Rough Fractures

Self-affine 3D fractures were numerically reproduced from a laboratory profilometer study, where the fractal exponent was varied to study the effect of surface roughness. To assess the spatial statistics of each domain, we first selected a stationary size (defined as a size where we observe spatial invariance of the statistic of interest around the domain). Figure 11 shows the process of selecting an adequate subsample and its verdict on stationarity. To speed the computation, the smaller stationary square (200x200) was selected for the spatial continuity analysis.

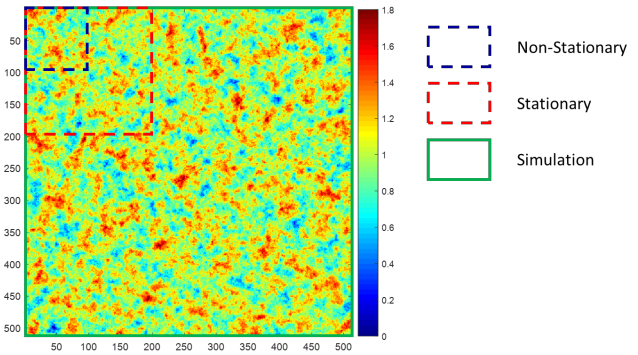

Figure 11: Different selections for stationarity check. The first square (blue) represents a domain size of 100x100, the next in size 200x200, following by the entire domain (512x512). The two later ones prove stationary.

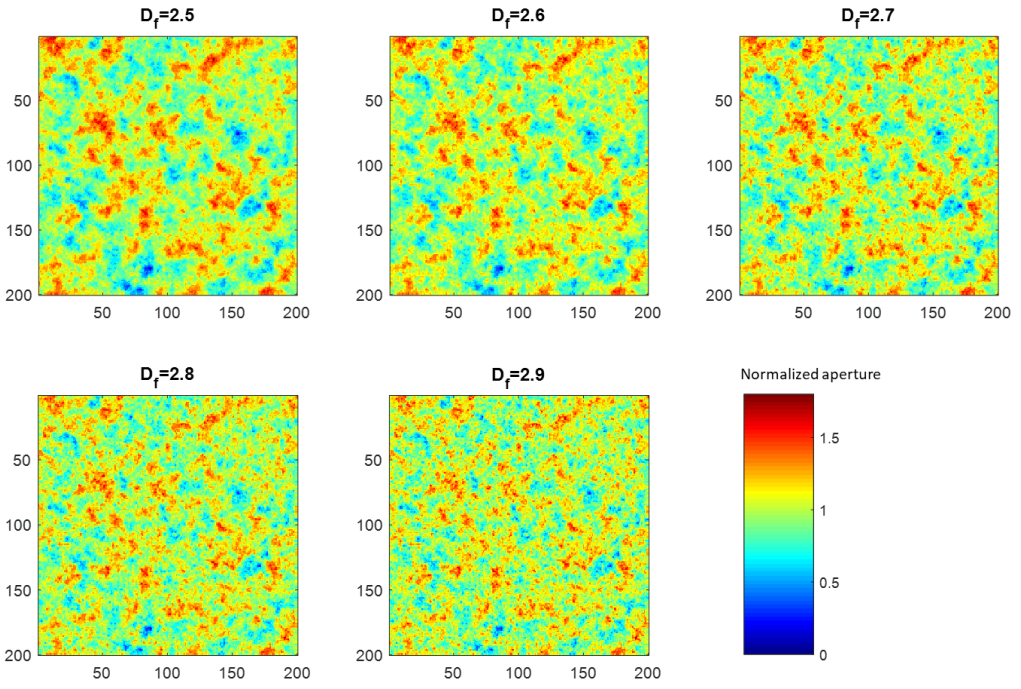

Figure 12: Fracture surfaces exhibiting increasing surface roughness. The fractal exponent (shown in bold) is used to define the amplitude of the Fourier component. The color map depicts normalized aperture.

To assess the spatial continuity of the fractures (and the size of our heterogeneities), an experimental variogram was calculated to the domains shown above. This diagram shows the degree of spatial self-dissimilarity. From Figure 13

we can see that an increase in the fractal dimension (roughness) yields in a higher nugget effect (short scale discontinuity), due to the local roughness. Where the smooth fracture exhibits almost 0%, the roughest displays a nugget effect close to 50%. It is also observed that these features cause a higher amount of residual saturation of the wetting phase (Figure 16). Another interesting feature is that the range of spatial correlation of the surfaces decreases with fractal exponent. The higher ranges give rise to a non-homogeneous front advance (Figure 14).

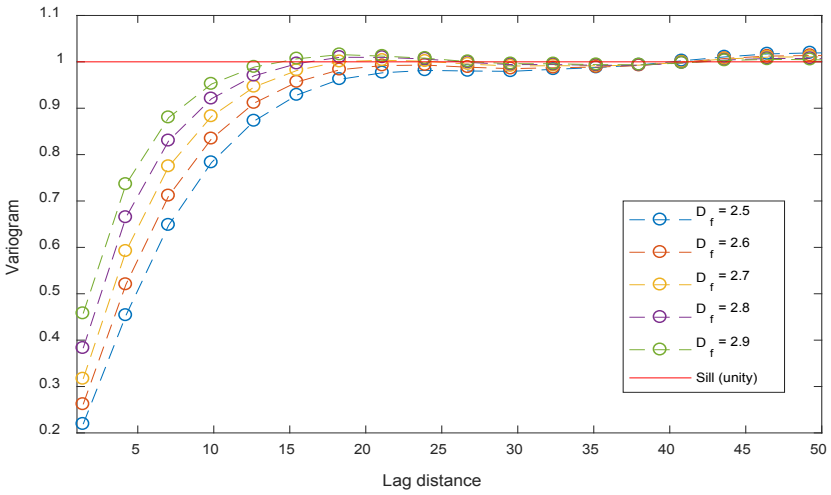

Figure 13: Isotropic variogram of the apertures for the 5 domains presented above, it is noticeable that the range changes with respect to the surface roughness. There are some published attempts in literature (Pyrcz & Deutsch, 2014), to relate the variogram range to the depositional setting.

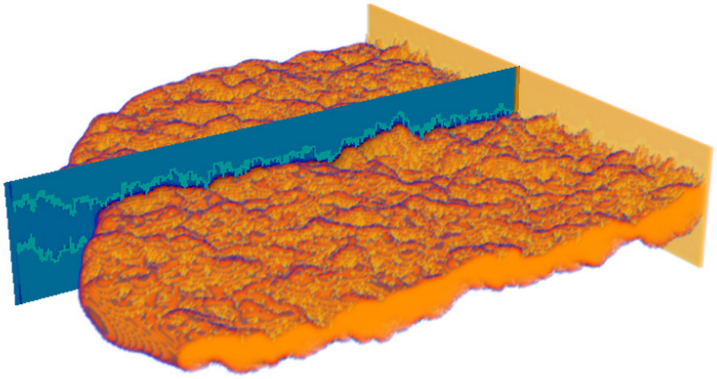

Figure 14: Drainage simulation for D_f=2.9. The blue cross section shows the fracture geometry. It is visible from the orange fluid (non-wetting) surface that wetting fluid remains trapped in the corners.

Table 3: For these cases, the geometrical ratio was selected as half of the variogram range, similar to the radius of the heterogeneities in Table 2.

$\mathbf{D_f}$	$\langle a \rangle / (\frac{1}{2}$ range)
2.5	0.47
2.6	0.73
2.7	1.48
2.8	1.93
2.9	2.66

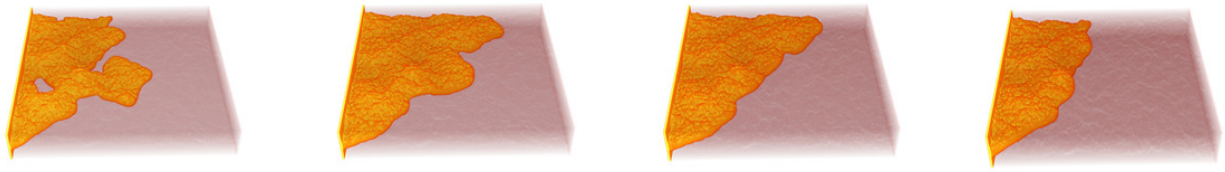

Figure 15: Comparison of the front advance for the fractures with D_f of 2.5, 2.6, 2.7 and 2.8. An increase on the homogeneity of the front is observed with the increase of the geometrical ratio displayed in Table 3.

As seen in the heterogeneously wetted cases, the invading front shape tends to be more homogeneous (Figure 15, right side) with an increase in the geometrical ratio. This increase also results in higher pressures to percolate the fracture (Figure 16), consequence of a more difficult pathway.

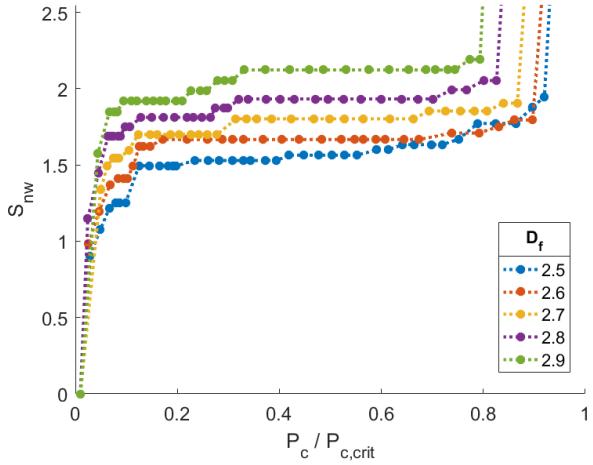

Figure 16: Capillary pressure-saturation curve for drainage of the different domains. The critical pressure was calculated with the average fracture aperture.

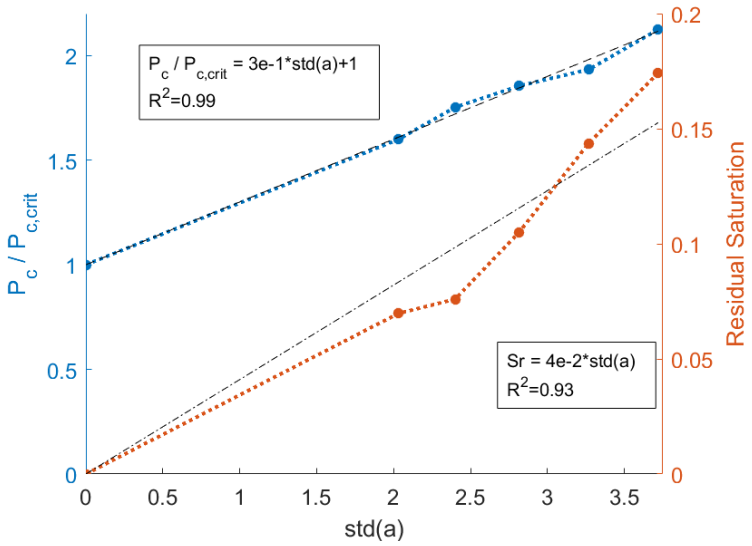

Figure 17: Normalized capillary pressure (left axis) and residual saturation (right axis) plot against standard deviation in aperture. The proposed models are shown in black dotted lines.

3.5 Flow through Rough Heterogeneous Fractures

Utilizing multipoint statistics (Strebelle, 2002), a mineralogy map was produced (Figure 18, left) based on a segmented SEM image used as a training input. The most relevant feature of the image, is that there is a phase connected across the domain (b) and an isolated one (a). It has been shown, that these images are appropriate to represent multiscale sources of information on a single domain (Gerke et al., 2015). To study the importance of connected structures, we carried out imbibition simulations in the roughest of our fractures (D_f=2.9, where the front shape was the most homogenous) mapping the wettability of the system with our stochastic realization.

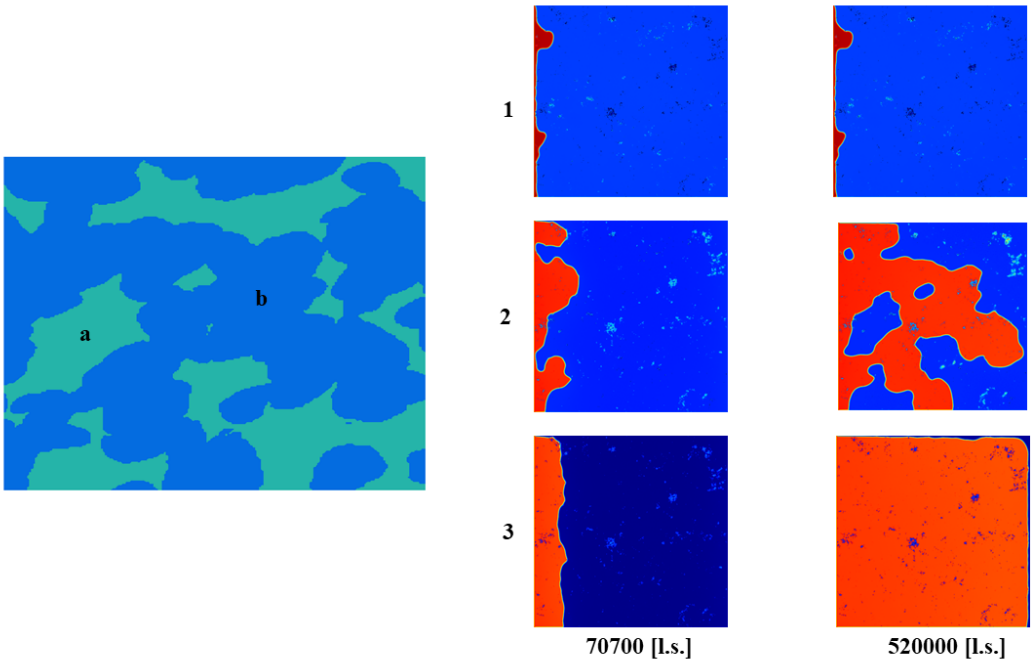

Figure 18: Imbibition tests at different times for 3 different rough domains. On the left, the mineralogy map is shown, where a and b refer to different mineralogy. On the right, three different cases are exemplified: 1) Patch a is wetting, b is non-wetting, 2) Patch a is non-wetting, b is wetting, 3) The entire surface is wetting. The images show a domain cross section, where on the invasive fluid is sown in red.

Simulations show that the wetting phase connectivity plays a critical role in fluid breakthrough. Even though the paths are more tortuous in Figure 18 (right), the imbibition front breaks through at the same time. Also, the fluid trapped in the corners (blue speckles on the red fluid), remains the same.

4. Conclusions

Direct simulations of drainage and imbibition were performed on realistic digitally reconstructed domains to assess the effect of surface heterogeneity. The influence of roughness (quantified by fractal dimension) and mineralogy was studied individually to evaluate the most relevant variables that affected multiphase flow displacements. It was found that the ratio of aperture over the heterogeneity size controls the formation of features such as fingers, contact line pinning and channeling; and cause steeper capillary pressure curves. It has been demonstrated that there is a threshold that characterizes the change in behavior.

To account for the size of the ‘aperture clusters’, an isotropic variogram was used. It is shown that higher fractal dimensions results in shorter spatial continuity. The domains exhibiting high spatial continuity displayed heterogeneous fronts due to the low geometrical ratio (less than 1). On the other hand, there is linear correlation of the standard deviation of apertures with trapped fluid fraction and capillary pressure increase. Clusters of trapped fluid are larger for smoother surface (if they exist), but the residual saturation in the overall domain is higher for the rougher domains.

Acknowledgments

We acknowledge the Texas Advanced Computing Center (TACC, **http://www.tacc.utexas.edu**) for providing high performance supercomputing clusters to run our simulations. M. P. and C. L. gratefully acknowledge the support from Shell-UT Unconventional Resources (SUTUR) program. J.E.S. would like to thank John Pederson for his valuable comments.

Nomenclature

a	fracture aperture
D_f	fractal dimension (related to the surface roughness)
$L_{w/nw}$	length of the intersection between the wetting and non-wetting patches in the surface
P_c	measured capillary pressure
$P_{c,crit}$	critical capillary pressure (pressure needed to drain a fully non-wetting domain, used for normalizing)
s	stripe width
w	domain length

References

Bear, J. (1993). *Flow and Contaminant Transport in Fractured Rock*.

Bhatnagar, P. L., Gross, E. P., & Krook, M. (1954). A model for collision processes in gases. I. Small amplitude processes in charged and neutral one-component systems. *Physical Review*, *94*(3), 511–525. https://doi.org/10.1103/PhysRev.94.511

Brown, S. R. (1995). Simple mathematical model of a rough fracture. *Journal of Geophysical Research: Solid Earth*, *100*(B4), 5941–5952. https://doi.org/10.1029/94JB03262

Brown, S. R., & Scholz, C. H. (1985). Broad bandwidth study of the topography of natural rock surfaces. *Journal of Geophysical Research*, *90*(B14), 12575. https://doi.org/10.1029/JB090iB14p12575

Cassie, A. B. D. (1948). Contact angles. *Discussions of the Faraday Society*, *3*, 11. https://doi.org/10.1039/df9480300011

Cheng, J. T., Pyrak-Nolte, L. J., Nolte, D. D., & Giordano, N. J. (2004). Linking pressure and saturation through interfacial areas in porous media. *Geophysical Research Letters*, *31*(8), 1–4. https://doi.org/10.1029/2003GL019282

Deglint, H. J., Ghanizadeh, A., Debuhr, C., & Clarkson, C. R. (2017). Comparison of Micro-and Macro-Wettability Measurements for Unconventional Reservoirs: The Devil is in the Detail. *Unconventional Resources Technology Conference*, (July), 24–26. https://doi.org/10.15530/urtec-2017-2690338

Dou, Z., Zhou, Z., & Sleep, B. E. (2013). Influence of wettability on interfacial area during immiscible liquid invasion into a 3D self-affine rough fracture: Lattice Boltzmann simulations. *Advances in Water Resources*, *61*, 1–11. https://doi.org/10.1016/j.advwatres.2013.08.007

Dupuis, A., & Yeomans, J. M. (2004). Lattice Boltzmann modelling of droplets on chemically heterogeneous surfaces. *Future Generation Computer Systems*, *20*, 993–1001. https://doi.org/10.1016/j.future.2003.12.012

Gale, J. F. W., Laubach, S. E., Olson, J. E., Eichhuble, P., & Fall, A. (2014). Natural Fractures in shale: A review and new observations. *AAPG Bulletin*, *98*(11), 2165–2216. https://doi.org/10.1306/08121413151

Gale, J. F. W., Reed, R. M., & Holder, J. (2007). Natural fractures in the Barnett Shale and their importance for hydraulic fracture treatments. *AAPG Bulletin*, *91*(4), 603–622. https://doi.org/10.1306/11010606061

Gerke, K. M., Karsanina, M. V., & Mallants, D. (2015). Universal stochastic multiscale image fusion: An example application for shale rock. *Scientific Reports*, *5*, 1–12. https://doi.org/10.1038/srep15880

Gneiting, T., & Schlather, M. (2001). Stochastic models which separate fractal dimension and Hurst effect, (1), 1–8. https://doi.org/10.1137/S0036144501394387

Hassanizadeh, S. M., & Gray, W. G. (1993). Thermodynamic basis of capillary pressure in porous media. *Water Resources Research*, *29*(10), 3389–3405. https://doi.org/10.1029/93WR01495

Huang, H., Thorne, D. T., Schaap, M. G., & Sukop, M. C. (2007). Proposed approximation for contact angles in Shan-and-Chen-type multicomponent multiphase lattice Boltzmann models. *Physical Review E - Statistical, Nonlinear, and Soft Matter Physics*, *76*(6), 1–6. https://doi.org/10.1103/PhysRevE.76.066701

Iglauer, S., Pentland, C. H., & Busch, A. (2015). CO 2 wettability of seal and reservoir rocks and the implications for carbon geo-sequestration. *Water Resources Research*, *51*(1), 729–774. https://doi.org/10.1002/2014WR015553

Iwahara, D., Shinto, H., Miyahara, M., & Higashitani, K. (2003). Liquid Drops on Homogeneous and Chemically Heterogeneous Surfaces: A Two-Dimensional Lattice Boltzmann Study. *Langmuir*, *19*(21), 9086–9093. https://doi.org/10.1021/la034456g

Jettestuen, E., Helland, J. O., & Prodanović, M. (2013). A level set method for simulating capillary-controlled displacements at the pore scale with nonzero contact angles. *Water Resources Research*, *49*(8), 4645–4661. https://doi.org/10.1002/wrcr.20334

Jung, N., Nadkarni, G. D., & Garoff, S. (1992). An Investigation of Microscopic Aspects of Contact Angle Hysteresis: Pinning of the Contact Line on a Single Defect Surfactant effects on droplet dynamics and deposition patterns: a lattice gas model An Investigation of Microscopic Aspects of Contact Angl. *Europhys. Lett*, *20*(6), 523–528. Retrieved from http://iopscience.iop.org/article/10.1209/0295-5075/20/6/009/pdf

Kusumaatmaja, H., & Yeomans, J. M. (2007). Modeling contact angle hysteresis on chemically patterned and superhydrophobic surfaces. *Langmuir*, *23*(11), 6019–6032. https://doi.org/10.1021/la063218t

Lake, L., Johns, R., Rossen, W., & Pope, G. (2014). *Fundamentals of enhanced oil recovery*. Retrieved from http://store.spe.org/Fundamentals-of-Enhanced-Oil-Recovery-Available-for-Pre-Order-P921.aspx

Landry, C. J., Karpyn, Z. T., & Ayala, O. (2014). Relative permeability of homogenous-wet andmixed-wet porousmedia as determined by pore-scale lattice Boltzmann modeling. *Water*, *50*(5), 3672–3689. https://doi.org/10.1002/2013WR015148.Received

Li, Q., Zhou, P., & Yan, H. J. (2016). Pinning-Depinning Mechanism of the Contact Line during Evaporation on Chemically Patterned Surfaces: A Lattice Boltzmann Study. *Langmuir*, *32*(37), 9389–9396. https://doi.org/10.1021/acs.langmuir.6b01490

Mandelbrot, B. B. (1983). *The fractal geometry of nature* (Vol. 173).

Ogilvie, S. R., Isakov, E., & Glover, P. W. J. (2006). Fluid flow through rough fractures in rocks. II: A new matching model for rough rock fractures. *Earth and Planetary Science Letters*, *241*(3–4), 454–465. https://doi.org/10.1016/j.epsl.2005.11.041

Pan, C., Hilpert, M., & Miller, C. T. (2004). Lattice-Boltzmann simulation of two-phase flow in porous media. *Water Resources Research*, *40*(1), 1–14. https://doi.org/10.1029/2003WR002120

Piri, M., & Karpyn, Z. T. (2007). Prediction of fluid occupancy in fractures using network modeling and x-ray microtomography. II: Results. *Physical Review E - Statistical, Nonlinear, and Soft Matter Physics*, *76*(1), 1–11. https://doi.org/10.1103/PhysRevE.76.016316

Prodanovic, M., & Bryant, S. L. (2009). Physics-Driven Interface Modeling for Drainage and Imbibition in

Fractures. *SPE Journal*, *14*(3), 11–14. https://doi.org/10.2118/110448-PA

Pruess, K., & Tsang, Y. W. (1990). On two-phase relative permeability and capillary pressure of rough-walled rock fractures. *Water Resources Research*, *26*(9), 1915–1926. https://doi.org/10.1029/WR026i009p01915

Pyrcz, M. J., & Deutsch, C. V. (2014). *Geostatistical Reservoir Modeling*. Oxford University Press.

Raeini, A. Q., Blunt, M. J., & Bijeljic, B. (2012). Modelling two-phase flow in porous media at the pore scale using the volume-of-fluid method. *Journal of Computational Physics*, *231*(17), 5653–5668. https://doi.org/10.1016/j.jcp.2012.04.011

Romm, E. S. (1966). Flow characteristics of fractured rocks. *Moscow*, (283).

Shan, X., & Chen, H. (1993). Lattice Boltzmann model for simulating flows with multi phases and components. *Physical Review E*, *47*(3), 1815–1819. https://doi.org/10.1103/PhysRevE.47.1815

Shan, X., & Chen, H. (1994). Simulation of nonideal gases and liquid-gas phase transitions by the lattice Boltzmann equation. *Physical Review E*, *49*(4), 2941–2948. https://doi.org/10.1103/PhysRevE.49.2941

Strebelle, S. (2002). Conditional Simulation of Complex Geological Structures Using Multiple-Point Statistics. *Mathematical Geology*, *34*(1), 1–21. https://doi.org/10.1023/A:1014009426274

Tokan-Lawal, A., Landry, C. J., Prodanovic, M., & Eichhubl, P. (2014). Understanding Tortuosity and Permeability variations in Naturally Fractured Reservoirs: Niobrara Formation. *Proceedings of the 2nd Unconventional Resources Technology Conference*, 1–13. https://doi.org/10.15530/urtec-2014-1922870

Tokan-Lawal, A., Prodanovic, M., & Eichhubl, P. (2015). Investigating flow properties of partially cemented fractures in Travis Peak Formation using image-based pore-scale modeling. *Journal of Geophysical Research B: Solid Earth*, *120*(8), 5453–5466. https://doi.org/10.1002/2015JB012045

Tokunaga, T. K., & Wan, J. (2013). Capillary Pressure and Mineral Wettability Influences on Reservoir CO2 Capacity. *Reviews in Mineralogy and Geochemistry*, *77*(1), 481–503. https://doi.org/10.2138/rmg.2013.77.14

Verma, R., Icardi, M., & Prodanović, M. (2018). Effect of wettability on two-phase quasi-static displacement: Validation of two pore scale modeling approaches. *Journal of Contaminant Hydrology*. https://doi.org/10.1016/J.JCONHYD.2018.01.002

Washburn, E. W. (1921). The Dynamics of Capillary Flow. *Physical Review*, *17*(3), 273–283. https://doi.org/10.1103/PhysRev.17.273

Zhang, J., Li, B., & Kwok, D. Y. (2009). Metastable contact angles and self-propelled drop movement on chemically heterogeneous surfaces by a mean-field lattice Boltzmann model. *European Physical Journal: Special Topics*, *171*(1), 73–79. https://doi.org/10.1140/epjst/e2009-01013-y